

Submitted to *Geophysics Research Letters* on October 7, 2010

1 **Terrestrial Myriametric Radio Burst Observed by *IMAGE* and**
2 ***Geotail* Satellites**

3

4 Shing F. Fung¹, Koza Hashimoto², Scott A. Boardsen³, Leonard N. Garcia⁴,

5 James L. Green⁵, Hiroshi Matsumoto⁶, and Bodo W. Reinisch⁷

6

7 ¹Geospace Physics Laboratory, NASA Goddard Space Flight Center, Greenbelt MD

8 ²Paleological Association of Japan, Inc., Kyoto, Japan

9 ³UMBC, NASA Goddard Space Flight Center, Greenbelt MD

10 ⁴Wyle, NASA Goddard Space Flight Center, Greenbelt MD

11 ⁵Planetary Science Division, NASA Headquarters, Washington D.C.

12 ⁶Headquarters, Kyoto University, Kyoto, Japan

13 ⁷Lowell Digisonde International, Lowell MA

14

15 ***Abstract***

16 We report *IMAGE* and *Geotail* simultaneous observations of a terrestrial myriametric
17 radio burst (*TMRB*) detected on August 19, 2001. The *TMRB* was confined in time (0830-
18 1006 UT) and frequency (12-50 kHz), suggesting a fan beam-like emission pattern from a
19 single discrete source. Analysis and comparisons with existing *TMR* radiations strongly
20 suggest that the *TMRB* is a distinct emission perhaps resulting from dayside magnetic
21 reconnection instigated by northward interplanetary field condition.

22

23 ***Introduction***

24 Myriametric radio emissions (with wavelengths of 10-100 km) from Earth's
25 magnetosphere have been known to take on different forms. Most notable forms include
26 the classical non-thermal continuum (*NTC*) with both escaping and trapped components,
27 continuum enhancement (*CE*), and auroral myriametric radiation (*AMR*). Continuum
28 radiation emanating from plasmaspheric notches at the magnetic equator can sometimes
29 extend to higher frequencies (up to ~ 800 kHz) to form the so-called kilometric
30 continuum (*KC*) radiation. *CE* has also been known to appear as low-frequency bursts
31 associated with substorm particle injections. This paper presents the simultaneous
32 *IMAGE* and *Geotail* observations of a burst of terrestrial myriametric radiation (*TMRB*) at
33 8:30-10:06 UT on August 19, 2001. The widely separated satellite observations at 12-50
34 kHz suggest that the *TMRB* was a temporal feature. We will compare the *TMRB*
35 observations to the characteristics of other known *TMR* components to determine if the
36 *TMRB* may be consistent with any of the known *TMR*.

37

38 ***Observations of Terrestrial Myriametric Radio Burst (TMRB)***

39 a) Spacecraft locations

40 On August 19, 2001, 0830-1006 UT, the *IMAGE* satellite was near apogee ($R \sim 8$ Re)
41 over the northern polar region in the afternoon sector while *Geotail* was at perigee ($R \sim 9$
42 Re) located just north of the magnetic equator in the post-midnight/pre-dawn sector.
43 Using the *NASA SSCWeb* tool (<http://sscweb.gsfc.nasa.gov>), we show in Figure 1 the
44 *IMAGE* and *Geotail* positions in *GSM* X-Y plane during the times of *TMRB* observations.

45 The *IMAGE* and *Geotail* *GSM* coordinates indicate that the two satellites were situated on
46 opposite sides of Earth, nearly along an afternoon-early morning meridian plane. *IMAGE*,
47 however, was at much-higher geomagnetic latitudes (71.81° - 80.46°) than *Geotail* (7.98° -
48 12.35°). The difference in geomagnetic longitudes shown in Figure 1 means that the two
49 satellites are situated on essentially diametrically opposite field lines. Over this interval,
50 the geomagnetic longitude of *IMAGE* changed by $\sim 11^{\circ}$, while that of *Geotail* was $\sim -5.3^{\circ}$.
51

52 b) *IMAGE* and *Geotail* observations

53 Figure 2 shows the 6-hour dynamic spectrograms for August 19, 2001, recorded by
54 the *IMAGE* Radio Plasma Imager (*RPI*, lower panel) [Reinisch *et al.*, 2000] and *Geotail*
55 Plasma Wave Instrument (*PWI*, upper panel) [Matsumoto *et al.*, 1994]. The emission
56 feature at 12-50 kHz observed simultaneously by both satellites at 0830-1006 UT
57 (demarcated by the two white lines) is identified here as the terrestrial myriametric radio
58 burst (*TMRB*). Given the widely separated spacecraft locations, the start and stop of the
59 *TMRB* being seen simultaneously by both satellites strongly suggest that the *TMRB* was
60 turning on and off, just like a light bulb.

61 In view of the differences in spacecraft locations, it is of interest to contrast the wave
62 signatures between the two spectrograms in Figure 2. Firstly, the *TMRB* observed by both
63 satellites appears as an isolated magnetospheric emission with an enhancement near the
64 center of the burst. The simultaneous observations of the *TMRB* when *IMAGE* and
65 *Geotail* were fortuitously located at different latitudes on diametrically opposite sides of
66 the Earth suggest that the *TMRB* must at a minimum have a fan-beam radiation pattern
67 that covers the latitude and longitude ranges of both *IMAGE* and *Geotail*. Broader

68 longitudinal beaming is possible in principle, but temporally extended *TMRB* emission
69 distinct from other *TMR* components (as discussed later) does not seem to be a common
70 occurrence, implying that *TMRB* may actually be limited in longitude.

71 Both *IMAGE* and *Geotail* detected several of the same solar type III bursts. One
72 burst was seen (near 7 UT) by *IMAGE* to have a low-frequency dispersive tail that
73 extends to the *TMRB* (Figure 2 lower panel) although no such tail was detected by
74 *Geotail* (Figure 2 upper panel). The absence of the type III tail at *Geotail* may be due to
75 its position at the time being deep in the night-side magnetosphere (see Figure 1) and that
76 the low-frequency tail might have been blocked by the dayside plasmasphere. The type
77 III tail seen at *IMAGE* location, however, means that the solar wind density at the time
78 must have been sufficiently low to allow the tail emission to penetrate the
79 magnetosphere. The solar wind plasma frequencies from *OMNI* data (white trace in the
80 upper panel of Figure 2) do show a near match of the lower cutoff of the first half of the
81 *TMRB*, but they quickly exceeded the *TMRB* lower cutoff throughout the rest of the burst.
82 This behavior essentially rules out the possibility of a solar wind source for the *TMRB*. In
83 addition, the observations of intensity enhancement near the burst center and distinct
84 upper frequency cutoffs by both *IMAGE* and *Geotail* argue strongly that the *TMRB* is a
85 distinct magnetospheric emission.

86 The start (0830 UT) and stop (1006 UT) of the *TMRB* were both observed practically
87 simultaneously at *IMAGE* and *Geotail* positions. While both the *IMAGE* and *Geotail*
88 observations show the same overall frequency extent (12-50 kHz) of the burst, they also
89 show that the burst has a lower cutoff frequency that decreases toward the center from
90 both the beginning and end of the burst. The frequency bandwidth is also broadest at the

91 center of the burst where *Geotail* observations seem to extend to slightly lower
92 frequencies. Both sets of observations clearly show no other connecting myriametric
93 radiation, so that the *TMRB* was an isolated emission.

94 Figure 3 shows an expanded view of the last hour of the *TMRB* in *Geotail* data (see
95 upper panel of Figures 2). The clearly spin-modulated burst signals shown in Figure 3
96 imply that the *TMRB* radiation was beamed directly from its source, although no such
97 spin-modulation was seen by *IMAGE RPI* due to the much slower satellite spin rate (0.5
98 RPM) and a longer time (~ 2 min) to complete a frequency scan. The tapered shape of the
99 frequency-time profile toward the end of the burst, particularly the lower cutoff
100 frequencies, is quite evident and consistent with the *IMAGE* observations shown in
101 Figure 2 lower panel. The upper cutoff frequencies, on the other hand, exhibit a number
102 of cycles of undulations, as if the source densities were going through a series of
103 enhancements and depletions.

104

105 ***Solar Wind and Magnetospheric Conditions Associated With the TMRB***

106 A number of terrestrial myriametric radiation components are dependent on
107 geomagnetic activity. It is therefore of interest to see what solar wind and auroral
108 conditions are associated with the *TMRB* emission.

109 *a) Solar wind conditions*

110 Figure 4 plots the 5-minute solar wind, interplanetary, and auroral activity data
111 obtained from the *NASA OMNIWeb* (<http://omniweb.gsfc.nasa.gov>). The top 3 panels in
112 Figure 4 show the interplanetary magnetic field (*IMF*) strength, *IMF* Bz (in *GSM*) and

113 solar wind speed, respectively. These parameters show no remarkable *IMF* activity
114 before and during the entire *TMRB* interval, with $3 < IMF |B| < 7$ nT and $+1 < IMF B_z <$
115 $+6$ nT. The solar wind speed in fact decreased rather steadily from 490 km s^{-1} at 0600 UT
116 to 450 km s^{-1} at 0900 UT. The positive *IMF* B_z condition throughout the interval,
117 however, may be of significance because magnetic reconnection can occur over limited
118 region poleward of the cusp [*e.g.*, *Kessel et al.*, 1996] and could potentially provide a
119 high-latitude free energy source to produce the *TMRB*.

120 b) *Auroral conditions*

121 The lower 4 panels in Figure 4 show the *AE*, *AL*, *AU*, and polar cap (*PC*) indices.
122 Due to the positive *IMF* B_z condition during this interval, there was also no remarkable
123 substorm activity. Nevertheless auroral kilometric radiation (*AKR*) was present at the
124 beginning and the second half of the *TMRB* interval. Referring to the panels in Figure 4
125 for the *AE*, *AL*, and *PC* indices, we notice that those indices exhibit peak levels around
126 0700, 0825, and 0940 UT, consistent with the times of *AKR* activations shown in Figures
127 2. On the other hand, Figure 4 shows no apparent auroral activation during the times of
128 *TMRB*. It would seem then that if an association were to exist between *TMRB* and *AKR*
129 (or auroral activity), the two emissions at different frequency ranges are not directly
130 correlated. Figure 2 suggests that *TMRB* tends to occur after *AKR* activation.

131

132 ***Comparisons of TMRB with known TMR Components***

133 The *TMRB* appeared in the same wavelength band (10-100 km) as other terrestrial
134 myriametric radiation. The most notable ones are the different forms of continuum

135 radiation [e.g., *Green and Fung, 2005; Grimald et al., 2008*] and the auroral myriametric
136 radiation [*Hashimoto et al., 1998*]. We now compare the observed characteristics of
137 *TMRB* against the known terrestrial emissions to see whether the *TMRB* might be a
138 distinct emission.

139 a) *Nonthermal continuum (NTC)*

140 Classical *nonthermal continuum radiation (NTC)* usually appears as banded emission
141 that extends several hours in the post-midnight to afternoon local times [*Gurnett, 1975;*
142 *Gough, 1982; Green and Boardsen, 1999; Menietti et al., 2005*]. In addition, trapped
143 *NTC* at frequencies below the magnetopause plasma frequency (~ 30 kHz) typically
144 appears as a broadband emission due to the radiation having undergone multiple
145 reflections within the magnetosphere [*Green and Fung, 2005*]. On the other hand, the
146 *TMRB* beam pattern is compact, limited both in latitude and longitude and/or time
147 (Figures 1, 2, and 3). Spin-modulations of *TMRB* shown in Figure 4 indicate that the
148 radiation detected by *Geotail* in the night-side magnetosphere was beamed directly from
149 the source.

150 Using ray-tracing calculations, *Green and Boardsen [1999]* showed that *NTC* is
151 primarily confined to low latitudes, and ray paths reflected off the magnetopause can
152 rarely pass over the polar region at $Z > 5$ Re. While these results are consistent with
153 *Geotail's* position during the *TMRB* observation, spectral differences from the *NTC* and
154 the detection of *TMRB* by *IMAGE* at high altitude ($Z > 7$ Re) over the high-latitude
155 region (see Figure 1) thus make the *TMRB* likely to be an emission distinct from the
156 classical *NTC*.

157 b) *Continuum enhancement (CE)*

158 Continuum enhancements are episodic *NTC* intensity enhancements that can last up
159 to ~ 2 hours [*Kasaba et al.*, 1998]. First identified in *GEOS 2* data taken in the
160 geosynchronous region near midnight [*Gough*, 1982], and then in *IMP 6* observations in
161 the magnetotail [*Filbert and Kellogg*, 1989], *CE* is characterized by a sudden
162 intensification at 15-30 kHz that is followed by an overall broadening to higher
163 frequencies and separating into discrete frequency bands (see Figure 3 in *Gough* [1982]).
164 The band separations also widen with time. The *TMRB* spectral appearance seems to
165 differ from *CE* by the lacking of clear frequency bands; but instead the upper cutoff
166 frequencies exhibit some undulations toward the end of the burst (Figure 3).

167 Onsets of *CE* are known to temporally correspond to increases in auroral activity
168 (*AE*, *AU*, and *AL*), including *AKR* [*Filbert and Kellogg*, 1989; *Kasaba et al.*, 1998]. As
169 shown in Figure 2, *AKR* and *TMRB* do not have matching start times. The times of
170 increases in auroral indices in Figure 4 are also inconsistent with the beginning time of
171 the *TMRB*. Despite the similarity in the compact spectral appearances in the *TMRB* and
172 the main *CE* component, the two emissions are not likely to be the same phenomenon.

173 c) *Kilometric continuum (KC)*

174 *TMRB* appears to be confined in latitude and longitude, similar to *KC* [*Green et al.*,
175 2004], but that might be the only similarities between the two emissions. Observed at all
176 local times, *KC* is generated from deep inside plasmaspheric notches that rotate with the
177 plasmasphere. The narrow latitudinal emission cone of *KC* ($\pm 15^\circ$ of the magnetic
178 equator) [*Green et al.*, 2004; *Hashimoto et al.*, 2006] can lead to different spectral
179 appearances that depend on the observing satellite orbital characteristics. First identified

180 in observations by *Geotail* in a near equatorial orbit [*Hashimoto et al.*, 1999], all the *KC*
181 discrete frequency bands lasted several hours due to the nearly synchronous changes in
182 the emission cone and spacecraft local times [*Green et al.*, 2002; 2004], see Figure 2.3 in
183 *Hashimoto et al.* [2006]. On the other hand, the polar-orbiting *IMAGE* satellite often
184 observed *KC* upon crossing the magnetic equator as discrete-banded emissions with
185 Christmas-tree patterns (*e.g.*, see Figure 2 in *Green and Boardsen*, [2006]). With the
186 Christmas-tree center frequencies extending up to ~ 800 kHz, the emission band
187 durations change from several hours at low frequencies (consistent with *Geotail*
188 observations) to less than an hour at high frequencies, yielding the Christmas-tree
189 spectral pattern. The very similar timing, frequency extents, and spectral shapes of the
190 *TMRB* observed by *Geotail* and *IMAGE* from very different vantage points (Figure 2)
191 mean that the *TMRB* reported here is distinct from *KC*.

192 d) *Auroral myriametric radiation (AMR)*

193 The *AMR*, first discussed by *Hashimoto et al.* [1994], gets its name because it occurs
194 coincidentally with *AKR* and substorm onsets. This emission is believed to be generated in
195 the *L-O* mode above the local plasma frequency (f_{pe}) in auroral density cavities where the
196 local electron gyrofrequency $f_{ce} > f_{pe}$. The difference in f_{ce} and f_{pe} naturally explains the
197 difference in *AKR* and *AMR* frequency ranges [*Hashimoto et al.*, 1998]. Although *AMR*
198 beaming can potentially account for the nightside *TMRB* observation by *Geotail*, it could
199 not easily explain the dayside observation at high latitude by *IMAGE*. The high temporal
200 correlation between *AMR* and *AKR* makes *AMR* an unlikely candidate for the observed
201 *TMRB* (Figure 2).

202

203 ***Summary and Conclusions***

204 We report the simultaneous observations of a terrestrial myriametric radio burst,
205 *TMRB*, by *Geotail* and *IMAGE* from very different vantage points (Figure 1). The
206 similarities in timing, frequency extents (12-50 kHz), and spectral characteristics of the
207 *TMRB* seen by the two spacecraft (Figures 2) imply that the *TMRB* was a temporal
208 emission with a fan beam radiation pattern emitted from a discrete source. The *TMRB*
209 upper cutoff frequencies appear to exhibit undulations as shown in Figure 3. Such
210 variability is reminiscent of the density increases and decreases as seen across field-
211 aligned density irregularities (*FAI*). For *L-O* mode propagation, the *TMRB* undulations
212 may suggest the presence of *FAI* in the *TMRB* source region.

213 The *TMRB* emission seems to occur only after *AKR* activation as shown in Figures 2
214 and 4, so its emission process might be a consequence of auroral activity. On the other
215 hand, the positive *IMF* *Bz* condition throughout the *TMRB* interval (Figure 4) suggests
216 that magnetic reconnection occurring over limited longitudinal range poleward of the
217 cusp could provide a transient, high-latitude free energy source at high altitude so that the
218 *TMRB* can be observed by *IMAGE* and *Geotail* from their respective locations (Figure1).
219 This is consistent with the compactness of the observed *TMRB* emission pattern.

220 Comparisons of *TMRB* characteristics against all other known *TMR* components
221 reveal that the *TMRB* was likely a distinct emission, although the emission mechanism
222 might still be the same as those responsible for generating the *NTC*, *CE*, *KC* or *AMR*. The
223 *TMRB* may thus be beamed radiation resulting from linear [Jones, 1976; Grimald et al.,
224 2007] or nonlinear mode-conversion mechanisms [e.g., Fung and Papadopoulos, 1987],
225 consistent with the spin-modulations seen by *Geotail*. We plan to validate this by

226 performing ray-tracing modeling of the *TMRB* propagation from potential source regions.

227

228 ***Acknowledgments***

229 We gratefully acknowledge the *SSCWeb* and *OMNIWeb* services provided by the *NASA*

230 *Space Physics Data Facility* and the use of the *OMNI* data sets.

231

232 ***References***

233 Filbert, P. C., and P. J. Kellogg (1989), Observations of low frequency radio emissions in

234 the Earth's magnetosphere, *J. Geophys. Res.*, **94**, 8867.

235

236 Fung, S.F. and K. Papadopoulos (1987), The emission of narrow-band Jovian kilometric

237 radiation, *J. Geophys. Res.* **92**, 8579–8593.

238

239 Gough, M.P., Nonthermal continuum emissions associated with electron injections:

240 Remote plasmopause sounding, *Planet. Space Sci.*, **30**, 657, 1982.

241

242 Green, J. L., and S. Boardsen (1999), Confinement of nonthermal continuum radiation to

243 low latitudes, *J. Geophys. Res.*, **104**, 10,307– 10,316.

244

245 Green, J. L. and S. Boardsen, Kilometric continuum radiation, *Radio Sci. Bull.*, URSI,

246 **318**, pp. 34-42, 2006.

247

248 Green, J. L. and S. F. Fung, Advances in Inner Magnetospheric Passive and Active Wave
249 Research, in *Physics and Modeling of the Inner Magnetosphere*, Geophysical Monogr.
250 155, AGU, Washington D.C., pp. 181-202, 2005.

251

252 Green, J. L., *et al.*, Association of kilometric continuum radiation with plasmaspheric
253 structures, *J. Geophys. Res.*, *109*, A03203, doi: 10.1029/2003JA010093, 2004.

254

255 Grimald, S., *et al.*, (2008), Medium-latitude sources of plasmaspheric nonthermal
256 continuum radiations observed close to harmonics of the electron gyrofrequency, *J.*
257 *Geophys. Res.*, *113*, A11216, doi:10.1029/2008JA013290.

258

259 Gurnett, D. A., The Earth as a radio source: The nonthermal continuum, *J. Geophys Res.*,
260 **80**, 2751-2763, 1975.

261

262 Hashimoto, K., *et al.*, Auroral myriametric radiation observed by Geotail, *Geophys Res.*
263 *Lett.*, **21**, 2927-2930, 1994.

264

265 Hashimoto, K., *et al.*, Source of auroral myriametric radiation observed with Geotail, *J.*
266 *Geophys. Res.*, **103**, 23475-23483, 1998.

267

268 Hashimoto, K., *et al.*, Kilometric continuum detected by GEOTAIL, *J. Geophys. Res.*,
269 **104**, 28,645– 28,656, 1999.

270

- 271 Hashimoto, K., *et al.*, Review of Kilometric continuum, in *Geospace Electromagnetic*
272 *Waves and Radiation*, ed. by J. W. LaBelle and R. A. Treumann, Lecture Notes in
273 Physics, vol. 687, Springer, Berlin, pp. 37-54, 2006.
274
- 275 Jones, D., W., Source of terrestrial non-thermal continuum radiation, *Nature*, **260**, 686-
276 689, 1976.
277
- 278 Kasaba, Y., *et al.*, Remote sensing of the plasmopause during substorms: GEOTAIL
279 observation of nonthermal continuum enhancement, *J. Geophys. Res.*, **103**, 20389-20405,
280 1998.
281
- 282 Kessel, R. L., *et al.*, Evidence of high-latitude reconnection during northward IMF:
283 Hawkeye observations, *Geophys. Res. Lett.*, **23**, 583-586, 1996.
284
- 285 Matsumoto, H., *et al.*, Plasma wave observations with *GEOTAIL* spacecraft, *J. Geomagn.*
286 *Geoelectr.* **46**, 59, 1994.
287
- 288 Meniatti, J. D., *et al.*, High resolution observations of continuum radiation, *Planetary and*
289 *Space Science*, **53**, 283–290, 2005.
290
- 291 Reinisch, B. W., *et al.*, The Radio Plasma Imager investigation on the *IMAGE* spacecraft,
292 *Space Science Reviews* special issue on the *IMAGE* mission, **91**, 319-359, 2000.
293
294

295
 297
 299
 301
 303
 305
 307
 309
 311
 313
 315
 317
 319
 321
 323
 325
 327
 328
 329
 330
 331
 332
 333

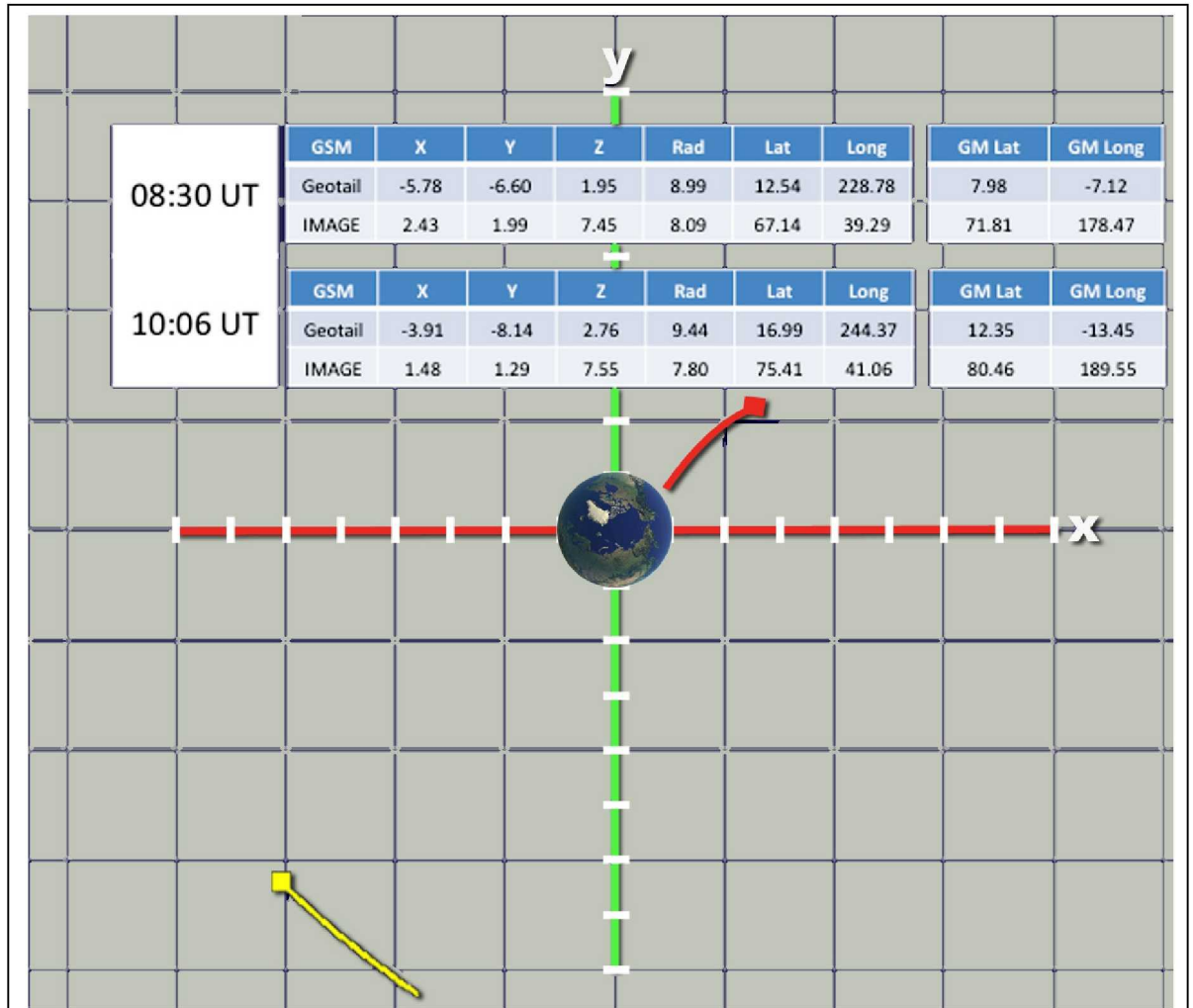


Figure 1. GSM and GM Positions of *IMAGE* (red) and *Geotail* (yellow) over the interval of *TMRB* observations on August 19, 2001. The two satellites were at different geomagnetic latitudes on opposite sides of the earth ($LT \sim 14.6$ and ~ 3.3 , respectively).

334

335

336

337

338

339

340

341

342

343

344

345

346

347

348

349

350

351

352

353

354

355

356

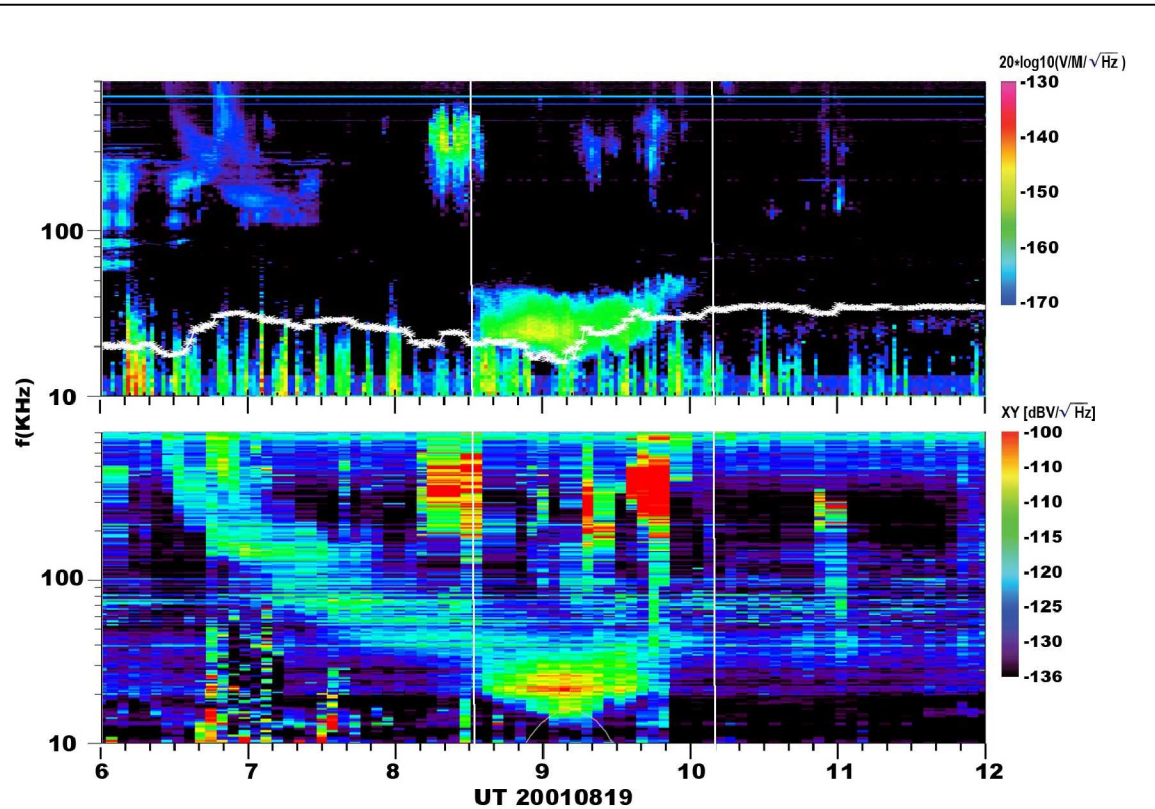


Figure 2. A 6-hour data interval showing the start and stop (demarcated by white lines) of the isolated *TMRB* being observed simultaneously by *IMAGE* on the dayside at high latitude (lower panel) and *Geotail* on the night side at low latitude (upper panel).

358

360

362

364

366

368

370

372

374

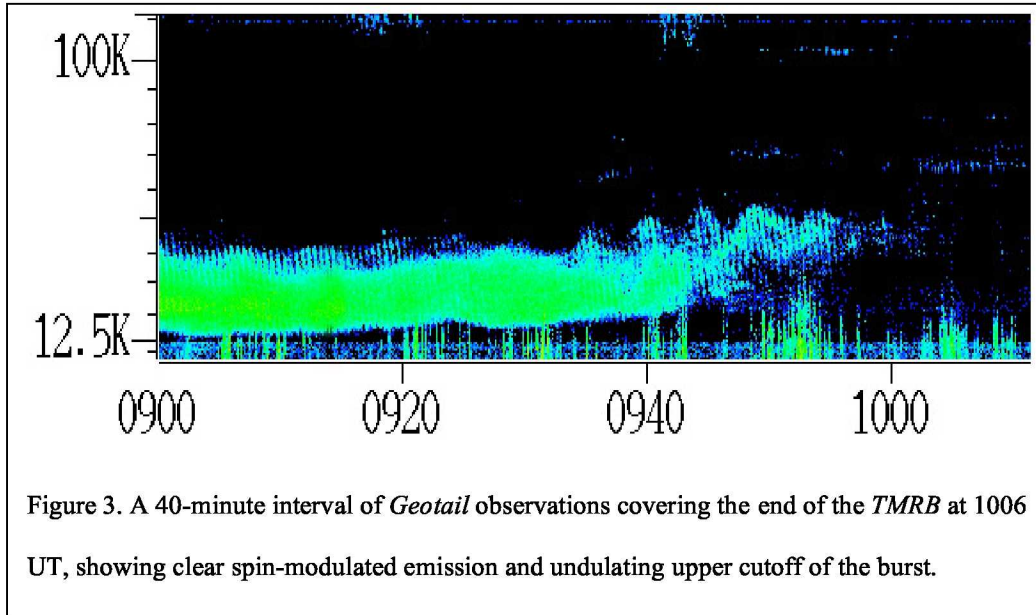


Figure 3. A 40-minute interval of *Geotail* observations covering the end of the *TMRB* at 1006 UT, showing clear spin-modulated emission and undulating upper cutoff of the burst.

376

378

380

382

384

386

388

390

392

394

396

398

400

402

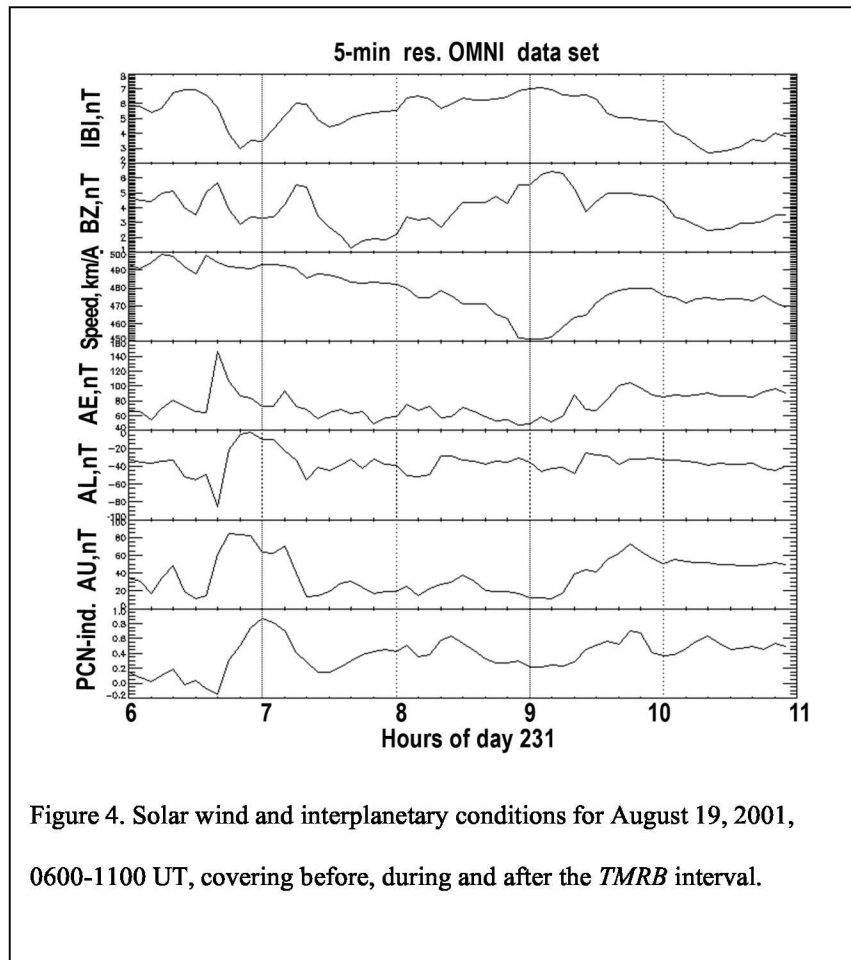


Figure 4. Solar wind and interplanetary conditions for August 19, 2001, 0600-1100 UT, covering before, during and after the *TMRB* interval.